

Collective Quantum Batteries and Charger-Battery Setup in Open Quantum Systems: Impact of Inter-Qubit Interactions, Dissipation, and Quantum Criticality

Mahima Yadav,^{1,*} Devvrat Tiwari,^{1,†} and Subhashish Banerjee^{1,‡}

¹*Indian Institute of Technology Jodhpur-342030, India*

(Dated: March 31, 2026)

Quantum batteries have emerged as promising platforms for exploring energy storage and transfer processes governed by quantum mechanical laws. In this work, we study three models of two-qubit open quantum systems. The first model comprises two central spins immersed in spin baths, and both central spins are collectively considered as quantum batteries. The impact of inter-qubit interactions on the performance of the quantum battery is investigated. In the second model, a two-qubit model interacting with a squeezed thermal bath serves as a collective quantum battery, where the impact of inter-atomic distance and the bath temperature on the battery's performance is explored. Furthermore, a two-qubit model is used, where one qubit is modeled as a battery and the other as a charger. The charger in this model interacts with an anisotropic spin-chain bath, which is conducive to quantum criticality. It is demonstrated that this criticality has a substantial impact on the quantum battery's storage capacity.

Keywords: Quantum thermodynamics, quantum battery, ergotropy, open quantum systems, central spin model

I. INTRODUCTION

Quantum thermodynamics provides a framework for understanding how the foundational laws of thermodynamics apply to quantum systems [1–8]. One of the primary objectives of this field is to correctly define the laws of thermodynamics governing energy exchange and entropy production in the quantum regime and understand the thermalization of quantum systems [9–12]. Recent advances have shown that exclusive quantum phenomena, such as entanglement and coherence, can act as thermodynamic resources [2, 13]. With the advancement in quantum technologies, quantum thermodynamics has been utilized in the development of various quantum thermal devices, ranging from heat engines [14–17], thermal analogs of electric devices [18], such as diodes [19], transistors [20, 21], adders [18], and Wheatstone bridges [18, 22], and quantum batteries [23–28], among others. Quantum batteries have recently garnered significant attention, demonstrating a quantum advantage in energy storage and transfer [29–31].

Quantum batteries are quantum mechanical systems designed to store energy temporarily for future use [23, 32–34]. The quantum battery can leverage the properties of a quantum system, such as coherence and entanglement, to gain an advantage in charging and power delivery rates [35, 36]. Quantum batteries have been realized on a number of platforms, including the Dicke model quantum battery with its extended Dicke model variant [37, 38], spin-chain quantum batteries [39, 40], strongly interacting Sachdev-Ye-Kitaev fermionic battery [41], solid-state quantum battery [37], self-discharge-mitigated quantum battery [42], resonator-qutrit quantum battery [43], Rosen-Zener quantum battery [44], topological quantum batteries [45], and Unruh-DeWitt battery [46], among others. The maximum amount of work that

can be extracted from a quantum battery is quantified by ergotropy [47]. In finite quantum systems, the passive state of a system (the state that can not perform work) is usually different from the Gibbs state and depends on the spectral decompositions of the state of the system and its Hamiltonian [48]. This can be further divided into its coherent and incoherent parts to accommodate the impact of population and coherence of a quantum state on ergotropy [49]. Further, the charging power is used to characterize the charging and discharging process of a quantum battery [26]. In realistic scenarios, the quantum battery—a quantum mechanical system—can not remain perfectly isolated from its ambient environment, and the environment has a significant impact on the work storage capacity of a quantum battery [26–28, 50–56].

The theory of open quantum systems accounts for the environmental effects on a quantum system [57–59]. Traditionally, the evolution of open quantum systems has been examined using the Markovian Gorini-Kossakowski-Sudarshan-Lindblad (GKSL) master equation [60, 61]. However, recently, rapid inroads have been made in the challenging domain of non-Markovian dynamics. The presence of non-Markovian evolution has been extensively explored and applied to various problems [62–68]. From the perspective of a quantum battery, non-Markovian evolution has been seen as a recharging mechanism, where the environment recharges the system after an initial discharge [26, 27, 51, 69].

The reservoir interacting with an open quantum system can be broadly classified into two types: a bosonic bath and a spin bath. The bosonic bath has been prototypical for a wide variety of open quantum systems, including the Caldeira-Leggett model and the spin-boson model, among others [70, 71]. The spin baths, composed of a finite number of spins, were initially observed in magnetic systems [72, 73]. Thereafter, this has been utilized in several systems and has been experimentally simulated using Rydberg atoms, quantum dots, and NV-centers, and has been incorporated into the experimental realization of a quantum battery [74–77]. The central spin model serves as the primary framework for studying spin baths [10, 78–82]. In a recent study, it has been demon-

* yadav.15@iitj.ac.in

† devvrat.1@iitj.ac.in

‡ subhashish@iitj.ac.in

strated that replacing the non-interacting spin-bath with an anisotropic spin-chain bath in a central spin model results in distinct critical behavior, leading to a quantum phase transition [83].

Quantum phase transitions, driven by quantum fluctuations, have drawn considerable interest [84–86]. Quantities such as entanglement, quantum speed limit time, and non-Markovianity have been found to be significantly impacted by these transitions [87–89]. It is imperative to study the impact of quantum critical behavior on the performance of a quantum battery.

In this work, we take up three two-qubit open quantum system models, two of which are envisaged as collective quantum batteries, and a charger-battery setup is modeled by the last one. The effects of inter-qubit interactions, dissipation by the bath, and quantum criticality on the performance of these quantum batteries are studied. Recently, quantum batteries have been realized with Dzyaloshinskii–Moriya (DM) interaction [90, 91] between the qubits [92–95]. Dipolar spin systems with coexisting dipole–dipole and DM interactions have also been explored to enhance quantum battery performance by exploiting quantum coherence [96]. This motivates us to compare the impact of inter-qubit interaction on a quantum battery. This is addressed using a two-qubit central spin model interacting with spin-baths [81, 82], where the two qubits are collectively considered as a quantum battery, and the impact of XXX [97–100] and DM inter-qubit interactions on its performance is compared. Furthermore, to explore the bath-assisted dissipation of the quantum battery, a two-qubit collective decoherence model interacting with a squeezed thermal bath is used. This model has been used to demonstrate entanglement generation between the qubits assisted by the bath, depending on the inter-qubit distance [101–103]. We investigate how this inter-qubit distance and the temperature of the bath affect the ergotropy of the collective two-qubit quantum battery. In a recent work, ergotropy and entanglement in interacting spin systems have been studied in the context of critical spin chains, illustrating how entanglement and system size affect extractable work in many-body spin models [104]. In this spirit, we explore the impact of quantum critical behavior on the dynamics of the quantum battery using a novel two-qubit central spin charger-battery setup. In this model, the charger qubit interacts with an anisotropic Heisenberg XY spin chain, and the battery is immersed in a non-interacting spin bath. This model demonstrates that criticality has a significant effect on the storage of charge in a quantum battery.

The plan of the paper is as follows. In Sec. II, we discuss the quantifiers used to investigate the performance of the battery and the models envisioned as a quantum battery. Section III discusses the impact of inter-qubit interactions on the collective central spin battery and inter-atomic distance, as well as bath temperature, on the two-qubit collective decoherence quantum battery. In Sec. IV, the central spin charger-battery setup is discussed, and the impact of quantum criticality on the battery’s performance is investigated. The conclusions are presented in Sec. V.

II. PRELIMINARIES

A. Characterizers of a quantum battery

To investigate the performance of a quantum battery, we use quantifiers such as ergotropy, energy, instantaneous, and average (dis-)charging powers, which are briefly discussed in this section.

1. Ergotropy

The ergotropy of a quantum system of dimension d , with the system Hamiltonian H_S and state $\rho_S(t)$ at any time t , is given by [47]

$$\mathcal{W}[\rho_S(t)] = \text{Tr}[\rho_S(t)H_S] - \text{Tr}[\rho_S^p(t)H_S], \quad (1)$$

where $\rho_S^p(t)$ is the passive state corresponding to the input state $\rho_S(t)$, from which no additional work can be extracted. The passive state is reached when the system undergoes an optimal unitary evolution driven by a cyclic potential. In contrast to macroscopic systems, where passive states typically coincide with thermal Gibbs states, the passive state of a finite-dimensional quantum system is in general distinct from a Gibbs state. The passive state for a microscopic quantum system is given by

$$\rho_S^p(t) = \sum_{j=1}^d r_j |\epsilon_j\rangle\langle\epsilon_j|, \quad (2)$$

where the $|\epsilon_j\rangle$ ’s come from the spectral decomposition of the system’s Hamiltonian $H_S = \sum_j \epsilon_j |\epsilon_j\rangle\langle\epsilon_j|$. The spectral decomposition of $\rho_S(t) = \sum_j r_j |r_j\rangle\langle r_j|$ is used to get the r_j ’s in the above equation. Importantly, the eigenvalues r_j and ϵ_j follow the order

$$r_1 \geq r_2 \geq r_3 \cdots \geq r_d, \quad \text{and} \quad \epsilon_1 \leq \epsilon_2 \leq \epsilon_3 \cdots \leq \epsilon_d. \quad (3)$$

The above ordering ensures that the lowest-energy state has the highest population, and as the level’s energy increases, its population decreases, making it passive with respect to work extraction.

The ergotropy can further be divided into coherent \mathcal{W}_c and incoherent ergotropy \mathcal{W}_i , such that $\mathcal{W} = \mathcal{W}_i + \mathcal{W}_c$ accommodating contributions of coherence and population terms of the system’s state [49]. The incoherent ergotropy is the amount of work that can be extracted from the system without altering its coherence by utilizing the dephased state of the system, and is given by

$$\mathcal{W}_i[\rho_S(t)] = \text{Tr}\left[\left\{\rho_S^D(t) - \rho_S^p(t)\right\}H_S\right], \quad (4)$$

where $\rho_S^D(t) = \sum_i \langle i|\rho_S(t)|i\rangle|i\rangle\langle i|$ denotes the dephased state for the system state $\rho_S(t)$, and $\rho_S^p(t)$ is the passive state corresponding to $\rho_S^D(t)$. The coherent ergotropy is then readily obtained as $\mathcal{W}_c[\rho_S(t)] = \mathcal{W}[\rho_S(t)] - \mathcal{W}_i[\rho_S(t)]$.

2. Energy and power

The energy of the system at any time t , using the Hamiltonian H_S and state of the system $\rho_S(t)$, is given by

$$E(t) = \text{Tr}[H_S \rho_S(t)]. \quad (5)$$

The corresponding instantaneous power of the system is defined as the time derivative of the energy, and is given by

$$P(t) = \frac{dE(t)}{dt}. \quad (6)$$

The energy and the power quantify the stored energy and its variation in the quantum battery. However, the amount of work that can be extracted from the quantum battery is quantified by ergotropy.

3. Charging power

Ergotropy is used to characterize the charging and discharging behavior of the quantum battery. The quantum battery is said to charge when ergotropy increases and to discharge when ergotropy decreases. The time derivative of ergotropy is the charging power given by

$$\mathcal{P}(t) = \frac{d\mathcal{W}[\rho_S(t)]}{dt}. \quad (7)$$

A quantum battery has a positive charging power when charging, whereas its charging power is negative when discharging. A zero charging power indicates that the battery is neither charging nor discharging. Further, for a single-qubit system, it has been shown that an interesting relationship exists between charging and instantaneous power, with both connected by a non-zero factor [28].

4. Average (dis-)charging power

The concept of average (dis-)charging power provides a useful measure of a quantum battery's performance over a given time interval. It is defined as the change in ergotropy during the period when the battery is being (dis-)charged, divided by the corresponding time duration during which the instantaneous charging power is negative (positive). Accordingly, the average (dis-)charging power over the interval $[t_i, t_f]$ can be expressed as

$$\bar{\mathcal{P}} = \frac{\mathcal{W}(t_f) - \mathcal{W}(t_i)}{t_f - t_i}. \quad (8)$$

Here, $\mathcal{W}(t_f)$ and $\mathcal{W}(t_i)$ denote the ergotropy at the final and initial times, respectively. This quantity indicates the net capacity with which the battery gains or loses its ergotropy, on average, over a given time interval.

B. Description of the models envisaged as a quantum battery

Here, we describe the models that specify the charger and the quantum battery, and categorize them based on different types of interaction.

1. A model of two central spins immersed in spin baths

We consider a model consisting of two coupled central spins (qubits), each interacting with its own local thermal spin bath, as in [81, 82]. The two baths are independent, that is, they do not interact with each other, and each bath is an ensemble of identical spins. The total system Hamiltonian H_{CS} is given by

$$H_{CS} = H_{S_1} + H_{S_2} + H_{S_1 S_2} + H_{B_1} + H_{B_2} + H_{S_1 B_1} + H_{S_2 B_2} \quad (9)$$

where $H_{S_l} = \frac{\hbar\omega_l}{2}\sigma_{l_z}^0$ ($l = 1, 2$), $H_{S_1 S_2} = \hbar V_{S_1 S_2}$, $H_{B_1} = \frac{\hbar\omega_a}{2M}\sum_{i=1}^M\sigma_{1z}^i$, $H_{B_2} = \frac{\hbar\omega_b}{2N}\sum_{i=1}^N\sigma_{2z}^i$, $H_{S_1 B_1} = \frac{\hbar\epsilon_1}{2\sqrt{M}}\sum_{i=1}^M(\sigma_{1x}^0\sigma_{1x}^i + \sigma_{1y}^0\sigma_{1y}^i)$, and $H_{S_2 B_2} = \frac{\hbar\epsilon_2}{2\sqrt{N}}\sum_{j=1}^N(\sigma_{2x}^0\sigma_{2x}^j + \sigma_{2y}^0\sigma_{2y}^j)$. Here, σ_{lk}^i or σ_{lk}^j ($k = x, y, z; l = 1, 2$) are the standard Pauli spin matrices corresponding to i -th or j -th spin of the l -th bath and σ_{lk}^0 ($k = x, y, z; l = 1, 2$) corresponds to the Pauli spin matrices for the l -th central spin. ω_1 and ω_2 are the transition frequencies of the two central spins. The interaction between the central spins is given by $V_{S_1 S_2}$, specified below. Further, ω_a and ω_b are the bath frequencies of the two spin baths, and ϵ_l 's are the uniform interaction strengths between the central spins and their corresponding spin baths. M and N are the number of spins in the two spin baths.

Now, using the collective angular momentum operators $J_{lk} = \frac{1}{2}\sum_i\sigma_{lk}^i$ (with $k = x, y, z; l = 1, 2$), the Hamiltonians describing the interaction between each central spin and its corresponding bath $H_{S_l B_l}$ can be rewritten as

$$\begin{aligned} H_{S_1 B_1} &= \frac{\hbar\epsilon_1}{\sqrt{M}}(\sigma_{1x}^0 J_{1x} + \sigma_{1y}^0 J_{1y}), \\ H_{S_2 B_2} &= \frac{\hbar\epsilon_2}{\sqrt{N}}(\sigma_{2x}^0 J_{2x} + \sigma_{2y}^0 J_{2y}), \end{aligned} \quad (10)$$

and the bath Hamiltonians H_{B_l} can be rewritten as

$$H_{B_1} = \hbar\omega_a \frac{J_{1z}}{M}, \quad \text{and} \quad H_{B_2} = \hbar\omega_b \frac{J_{2z}}{N}. \quad (11)$$

Considering the joint initial state of the system and bath as $\rho_{SB}(0) = \rho_{S_1 S_2}(0) \otimes \rho_{B_1}(0) \otimes \rho_{B_2}(0)$ (where thermal Gibbs state $\rho_{B_l}(0) = e^{-\beta_l H_{B_l}} / \text{Tr}[e^{-\beta_l H_{B_l}}]$ is taken as the initial state of each bath), we find the reduced dynamics of the two central spin system using the unitary evolution of the joint system bath

$$\rho_{S_1 S_2} = \text{Tr}_{B_1 B_2}(e^{-iH_{CS}t/\hbar}\rho_{SB}(0)e^{iH_{CS}t/\hbar}). \quad (12)$$

We shall analyze this model by considering two distinct types of interactions $V_{S_1 S_2}$ between the central spins. The first is the Heisenberg XXX interaction [97–100] $V_{S_1 S_2}^{\text{XXX}} =$

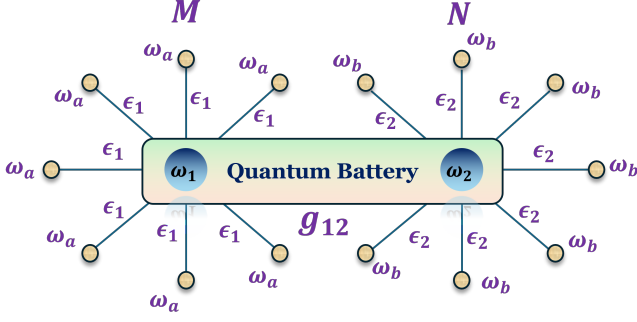


FIG. 1. A schematic diagram of the two-qubit collective central spin quantum battery.

$g_{12}(\sigma_{1x}^0 \otimes \sigma_{2x}^0 + \sigma_{1y}^0 \otimes \sigma_{2y}^0 + \sigma_{1z}^0 \otimes \sigma_{2z}^0)$. The second is the antisymmetric Dzyaloshinskii–Moriya (DM) interaction [90, 91], given by $V_{S_1 S_2}^{\text{DM}} = g_{12,z}(\sigma_{1x}^0 \otimes \sigma_{2y}^0 - \sigma_{1y}^0 \otimes \sigma_{2x}^0) + g_{12,x}(\sigma_{1y}^0 \otimes \sigma_{2z}^0 - \sigma_{1z}^0 \otimes \sigma_{2y}^0) + g_{12,y}(\sigma_{1z}^0 \otimes \sigma_{2x}^0 - \sigma_{1x}^0 \otimes \sigma_{2z}^0)$, where $g_{12,x} = g_{12,y} = g_{12,z} = g_{12}$ denotes the strength of the interaction. The two types of interaction are chosen to observe the effect of a symmetric and anti-symmetric exchange between the qubits of the batteries.

In this model, the two central spins are collectively envisioned as a quantum battery, see Fig 1, and their corresponding spin baths act as a dissipator or charger. Due to this, we call this setup a two-qubit collective central spin battery. The impact of both the XXX and DM interactions on the performance of this quantum battery is analyzed in Sec. III A.

2. Two qubit collective decoherence model

Here, a dissipative interaction model of two qubits (two-level atomic system) interacting with the squeezed bath [102] via dipole interaction [103] is considered. The Hamiltonian of the total system is given by [102, 103]

$$\begin{aligned} H_{\text{TQCD}} &= H_S + H_B + H_{SB} \\ &= \frac{1}{2} \sum_{l=1}^2 \hbar \omega_l \sigma_l^z + \sum_{\vec{k}s} \hbar \omega_k \left(b_{\vec{k}s}^\dagger b_{\vec{k}s} + \frac{1}{2} \right) \\ &\quad - i\hbar \sum_{\vec{k}s} \sum_{l=1}^2 \left[\vec{\mu}_l \cdot \vec{g}_{\vec{k}s}(\vec{r}_l) (\sigma_l^+ + \sigma_l^-) b_{\vec{k}s} - h.c. \right], \end{aligned} \quad (13)$$

where H_S , H_B , and H_{SB} are the system, bath, and system-bath interaction Hamiltonians, respectively, and $\sigma_l^+ = \frac{1}{2}(\sigma_l^x + i\sigma_l^y) = |e_l\rangle\langle g_l|$ and $\sigma_l^- = \frac{1}{2}(\sigma_l^x - i\sigma_l^y) = |g_l\rangle\langle e_l|$ are the standard atomic raising and lowering operators corresponding to qubit l . ω_l is transition frequency for qubit l . The transition dipole moments $\vec{\mu}_l$ depend on the atomic positions \vec{r}_l . The operators $b_{\vec{k}s}^\dagger$ and $b_{\vec{k}s}$ are the bosonic creation and annihilation operators, respectively, for the bath (field) mode $\vec{k}s$ with the wave vector \vec{k} , polarization index ($s = 1, 2$), and frequency ω_k . The system-bath (S-B) coupling constant is given

by [102, 103]

$$\vec{g}_{\vec{k}s}(\vec{r}_l) = \left(\frac{\omega_k}{2\epsilon\hbar V} \right)^{\frac{1}{2}} \vec{e}_{\vec{k}s} e^{i\vec{k}\cdot\vec{r}_l},$$

where V is the normalization volume and $\vec{e}_{\vec{k}s}$ is the unit polarization vector of the field. The density matrix describing the reduced dynamics of the system, using Born-Markov and rotating wave approximations, is given by the master equation of the form [102, 103]

$$\begin{aligned} \frac{d\rho}{dt} &= -\frac{i}{\hbar} [\tilde{H}_S, \rho] \\ &\quad - \frac{1}{2} \sum_{i,j=1}^2 \Gamma_{ij} [1 + \tilde{N}] (\rho \sigma_i^+ \sigma_j^- + \sigma_i^+ \sigma_j^- \rho - 2\sigma_j^- \rho \sigma_i^+) \\ &\quad - \frac{1}{2} \sum_{i,j=1}^2 \Gamma_{ij} \tilde{N} (\rho \sigma_i^- \sigma_j^+ + \sigma_i^- \sigma_j^+ \rho - 2\sigma_j^+ \rho \sigma_i^-) \\ &\quad + \frac{1}{2} \sum_{i,j=1}^2 \Gamma_{ij} \tilde{M} (\rho \sigma_i^+ \sigma_j^+ + \sigma_i^+ \sigma_j^+ \rho - 2\sigma_j^+ \rho \sigma_i^+) \\ &\quad + \frac{1}{2} \sum_{i,j=1}^2 \Gamma_{ij} \tilde{M}^* (\rho \sigma_i^- \sigma_j^- + \sigma_i^- \sigma_j^- \rho - 2\sigma_j^- \rho \sigma_i^-), \end{aligned} \quad (14)$$

where

$$\tilde{N} = N_{th}(\cosh^2(r) + \sinh^2(r)) + \sinh^2(r), \quad \text{and} \quad (15)$$

$$\tilde{M} = -\frac{1}{2} \sinh(2r) e^{i\Phi} (2N_{th} + 1) \equiv R e^{i\Phi(\omega_0)}, \quad (16)$$

with $\omega_0 = \frac{\omega_1 + \omega_2}{2}$. $N_{th} = \frac{1}{e^{\frac{\hbar\omega_0}{k_B T}} - 1}$ describes the Planck distribution, providing the number of thermal photons at the frequency ω and r, Φ are the squeezing parameters. The squeezed reservoir is assumed to be broadband, with squeezing bandwidths much larger than the atomic linewidths, such that the squeezing can be treated as frequency independent in the vicinity of the system transition frequency ω_0 . The carrier frequency of the squeezed field is taken to be resonant with the atomic transition. The explicit form of the system Hamiltonian used in Eq. (14) is given by [102, 103]

$$\tilde{H}_S = \frac{\hbar}{2} \sum_{l=1}^2 \omega_l \sigma_l^z + \hbar \sum_{i,j} \Omega_{ij} \sigma_i^+ \sigma_j^-, \quad (17)$$

where

$$\begin{aligned} \Omega_{ij} &= \frac{3}{4} \sqrt{\Gamma_i \Gamma_j} \left[-\left\{ 1 - (\hat{\mu} \cdot \hat{r}_{ij})^2 \right\} \frac{\cos(k_0 r_{ij})}{k_0 r_{ij}} \right. \\ &\quad \left. + \left\{ 1 - 3(\hat{\mu} \cdot \hat{r}_{ij})^2 \right\} \left\{ \frac{\sin(k_0 r_{ij})}{(k_0 r_{ij})^2} + \frac{\cos(k_0 r_{ij})}{(k_0 r_{ij})^3} \right\} \right], \end{aligned} \quad (18)$$

with $\hat{\mu} = \hat{\mu}_1 = \hat{\mu}_2$ being the unit vectors along the atomic transition dipole moments and \hat{r}_{ij} is the unit vector along $\vec{r}_{ij} = \vec{r}_i - \vec{r}_j$. Also, $k_0 = \omega_0/c$ and $r_{ij} = |\vec{r}_{ij}|$. The wave vector is given by $k_0 = \frac{2\pi}{\lambda_0}$, where λ_0 is the resonant wavelength. The term $k_0 r_{ij} \sim \frac{r_{ij}}{\lambda_0}$ in the above equation denotes a

ratio between the interqubit distance and the resonant wavelength. This term classifies the system's dynamics into two distinct regimes: independent and collective decoherence. In the independent decoherence regime, where $k_0 r_{ij} \geq 1$, each qubit experiences the environment independently. Conversely, as $k_0 r_{ij} \rightarrow 0$, the qubits are sufficiently close to each other, experiencing the environment collectively, thus referred to as the collective decoherence regime. Essentially, in the collective decoherence regime, the bath's correlation length, determined by λ_0 , is longer than the distance between the qubits, r_{ij} . Further, in the above equation, the spontaneous emission rate Γ_i is given by

$$\Gamma_i = \frac{\omega_i^3 \mu_i^2}{3\pi\epsilon\hbar c^3}, \quad (19)$$

while $\Gamma_{ij} = \Gamma_{ji} = \sqrt{\Gamma_i \Gamma_j} F(k_0 r_{ij})$, where $i \neq j$ with

$$F(k_0 r_{ij}) = \frac{3}{2} \left[\left\{ 1 - (\hat{\mu} \cdot \hat{r}_{ij})^2 \right\} \frac{\sin(k_0 r_{ij})}{k_0 r_{ij}} + \left\{ 1 - 3(\hat{\mu} \cdot \hat{r}_{ij})^2 \right\} \left\{ \frac{\cos(k_0 r_{ij})}{(k_0 r_{ij})^2} - \frac{\sin(k_0 r_{ij})}{(k_0 r_{ij})^3} \right\} \right].$$

Γ_{ij} 's represent collective spontaneous emission rates arising from the dissipative interaction of the multi-qubit system with the environment.

The two qubits are collectively modeled as a quantum battery, with the environment serving as a dissipator. To this effect, we coin the term for this battery as the collective decoherence battery. The impact of the inter-atomic distance and the temperature of the bath on the quantum battery using ergotropy and their (in-)coherent parts is investigated in Sec. III B.

3. Two central spin model in a charger-battery setup

The system consists of two central spins coupled to different spin baths. In this model, a central spin is modeled as a charger H_C and is coupled to a spin-chain bath H_{E_C} , consisting of N spins with nearest-neighbor interactions and an external magnetic field. The other central spin acts as a battery H_B surrounded by a non-interacting spin bath H_{E_B} , consisting of M spins, see Fig. 2. The total Hamiltonian for this model is given by

$$H_{C,B,E_C,E_B} = H_C + H_B + H_{CB} + H_{E_C} + H_{E_B} + H_{CE_C} + H_{BE_B}, \quad (20)$$

where (for $\hbar = 1$)

$$\begin{aligned} H_C &= \frac{\omega_C}{2} \sigma_C^z, \quad H_B = \frac{\omega_B}{2} \sigma_B^z, \quad H_{CB} = g_{CB} (\sigma_C^x \sigma_B^x + \sigma_C^y \sigma_B^y), \\ H_{E_C} &= \frac{\omega_{E_C}}{2} \sum_{l=1}^N \left[\left(\frac{1+\gamma}{2} \right) \sigma_l^x \sigma_{l+1}^x + \left(\frac{1-\gamma}{2} \right) \sigma_l^y \sigma_{l+1}^y - \lambda \sigma_l^z \right], \\ H_{E_B} &= \frac{\omega_{E_B}}{2} \sum_{k=1}^M \sigma_k^z, \quad H_{CE_C} = g_{CE_C} \sum_{l=1}^N (\sigma_C^x \sigma_l^x + \sigma_C^y \sigma_l^y), \\ H_{BE_B} &= g_{BE_B} \sum_{k=1}^M (\sigma_B^x \sigma_k^x + \sigma_B^y \sigma_k^y). \end{aligned} \quad (21)$$

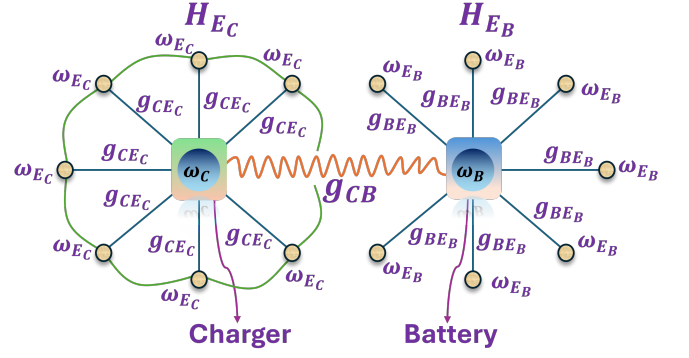


FIG. 2. A schematic diagram of two central spins in a charger-battery setup.

Here, H_C and H_B are the system Hamiltonians for the charger and the battery qubits, respectively, and H_{E_C} is the bath Hamiltonian surrounding the charger and H_{E_B} is the bath Hamiltonian surrounding the battery. Notably, the Hamiltonian for the bath surrounding the battery can be rewritten using the collective angular momentum operator $J_z = \frac{1}{2} \sum_k \sigma_k^z$ as $H_{E_B} = \omega_{E_B} J_z$. The environment interacting with the charger H_{E_C} is considered to be an anisotropic XY spin-chain with the anisotropic parameter γ , and λ characterizes the strength of the transverse magnetic field applied in the z direction. It should be noted that the last spin of the chain interacts with the first one, forming a closed spin chain. Furthermore, the interaction between the charger and battery is modeled by the Heisenberg XX interaction given by the Hamiltonian H_{CB} with strength g_{CB} . The interaction Hamiltonian between the charger and its environments is given by H_{CE_C} (with interacting strength g_{CE_C}), and that between the battery and its environment is given by H_{BE_B} (with interaction strength g_{BE_B}). The transition frequencies for the battery and charger are given by ω_B and ω_C , respectively, and ω_{E_C} and ω_{E_B} are the transition frequencies of the bath spins in the baths surrounding the charger and the battery.

The initial state of the composite system is taken to be $\rho(0) = \rho_C(0) \otimes \rho_B(0) \otimes \rho_{E_C}(0) \otimes \rho_{E_B}(0)$. The initial state of the bath surrounding the charger (battery) $E_{C(B)}$ is taken to be the thermal state at temperature $T_{C(B)}$, that is,

$$\rho_{E_{C(B)}}(0) = \frac{\exp(-H_{E_{C(B)}}/T_{C(B)})}{\text{Tr}[\exp(-H_{E_{C(B)}}/T_{C(B)})]}. \quad (22)$$

The reduced state of the charger-battery system is obtained by partially tracing their respective baths from the total dynamics as

$$\rho_{CB}(t) = \text{Tr}_{E_C, E_B} [U_{C,B,E_C,E_B} \{\rho(0)\} U_{C,B,E_C,E_B}^\dagger], \quad (23)$$

where $U_{C,B,E_C,E_B} = \exp(-iH_{C,B,E_C,E_B}t)$. Further, the reduced state of the battery at any time t is given by $\rho_B(t) = \text{Tr}_C[\rho_{CB}(t)]$. In principle, the initial states of both the charger and the battery can be taken arbitrarily. However, here, we

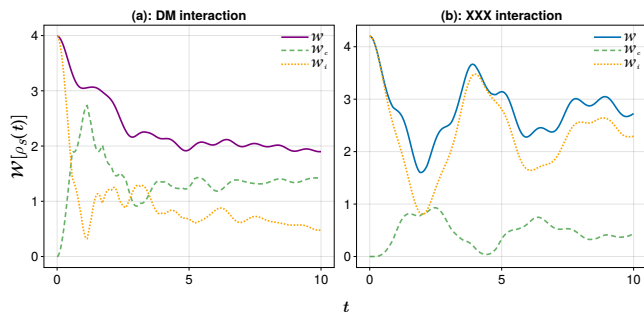


FIG. 3. Variation of the ergotropy $\mathcal{W}[\rho_S(t)]$, coherent ergotropy $\mathcal{W}_c[\rho_S(t)]$, and incoherent ergotropy $\mathcal{W}_i[\rho_S(t)]$ with time (in natural units, where $\hbar = k_B = 1$) for the two central spin quantum battery for both (a) DM and (b) Heisenberg XXX inter-qubit interactions. The parameters are taken to be: $\omega_1 = 1.15, \omega_2 = 1.25, \omega_a = 1.1, \omega_b = 1.2, g_{12} = 0.75, \epsilon_1 = \epsilon_2 = 0.5, \beta_a = 4, \beta_b = 1$, and $M = N = 8$.

consider the initial states of the charger and the battery as

$$\rho_C(0) = \begin{pmatrix} 1 & 0 \\ 0 & 0 \end{pmatrix}, \quad \rho_B(0) = \begin{pmatrix} 1/2 & 1/2 \\ 1/2 & 1/2 \end{pmatrix}, \quad (24)$$

respectively.

III. COLLECTIVE CHARGING AND DISCHARGING BEHAVIOR

Here, we consider the two-spin models discussed above and study the corresponding charging and discharging behavior. Both the spins in this scenario serve as a quantum battery, and their corresponding environment acts as a dissipating or recharging mechanism.

A. Two-qubit collective central spin battery

We model the interaction between the two central spins using two different types of interactions, see Sec. II B 1. In the first case, the interaction between the two central spins is governed by the Heisenberg XXX interaction, and in the second case, the two central spins interact via the DM interaction, see below Eq. (12). Initially, the system is considered to be in the excited state $|00\rangle$, where, in the computational basis, $|0\rangle = \begin{pmatrix} 1 \\ 0 \end{pmatrix}$ and $|1\rangle = \begin{pmatrix} 0 \\ 1 \end{pmatrix}$ denote the excited and ground state of the system, respectively. Using the initial state of the system, we calculate the reduced state of the two-qubit central spin model as given by Eq. (12). The ergotropy, Eq. (1), at each point of time, is calculated using this state of the system, and is depicted in Fig. 3. It can be observed that the ergotropy decreases rapidly for the XXX interaction compared to the DM interaction, indicating a quicker initial discharge of the system for this interaction. However, the recharging, facilitated by the corresponding spin baths, helps regain the ergotropy for the XXX interaction, which takes higher values

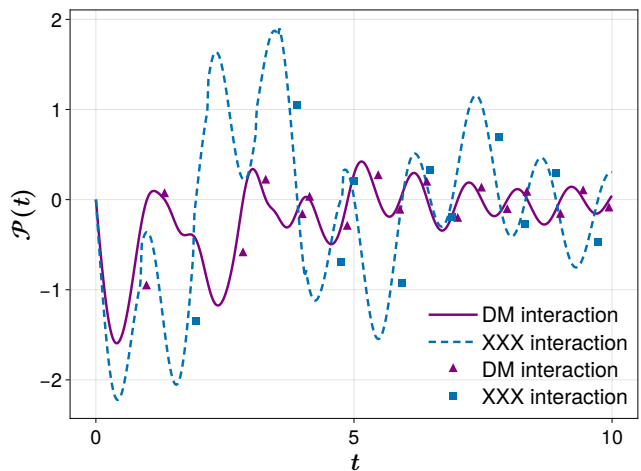


FIG. 4. Variation of the charging power $\mathcal{P}(t)$, Eq. (7), and average (dis-)charging power $\bar{\mathcal{P}}$, Eq. (8), with time (in natural units, where $\hbar = k_B = 1$) for the two central spin quantum battery for both DM and Heisenberg XXX interactions. The triangle and square markers show the average (dis-)charging power for DM and XXX inter-qubit interactions, respectively. The parameters are taken to be: $\omega_1 = 1.15, \omega_2 = 1.25, \omega_a = 1.1, \omega_b = 1.2, g_{12} = 0.75, \epsilon_1 = \epsilon_2 = 0.5, \beta_a = 4, \beta_b = 1$, and $M = N = 8$.

than the ergotropy for the DM interaction. This highlights that even though the battery discharges quickly when XXX interaction is present, it recharges and maintains a higher amount of work that can be extracted from it. The coherent and incoherent parts of the ergotropy are further plotted for both DM and XXX interactions in Figs. 3(a) and 3(b), respectively. In the case of the XXX interaction, the incoherent ergotropy contributes significantly to the ergotropy. In contrast, in the case of DM interaction, which is an antisymmetric, spin-orbit-type exchange [105], redistribution of populations toward lower-energy eigenstates occurs more rapidly, and hence the incoherent ergotropy remains lower. Later, the coherent ergotropy is the major contributor to the ergotropy in this case. This illustrates that the higher incoherent ergotropy is the reason behind a greater overall ergotropy for XXX inter-qubit interaction. The corresponding charging power $\mathcal{P}(t)$, Eq. (7), and average (dis-)charging power $\bar{\mathcal{P}}$, Eq. (8), for both types of inter-qubit interactions are plotted in Fig. 4. The positive charging power indicates charging of the quantum battery, and the discharging is indicated by the negative charging power. Furthermore, the average charging power is denoted by the corresponding markers with positive values, while the negative-valued markers depict the average discharging power. The charging power for the XXX inter-qubit interaction initially takes higher negative values, indicating that it discharges more compared to the DM inter-qubit interactions. However, the charging power also takes higher positive values for XXX interaction, illustrating that it can deliver more work at these times than the battery with DM inter-qubit interactions. The battery with XXX interaction also has a higher average (dis-)charging power. This highlights that, on average, the battery with XXX interaction can deliver more power than the battery

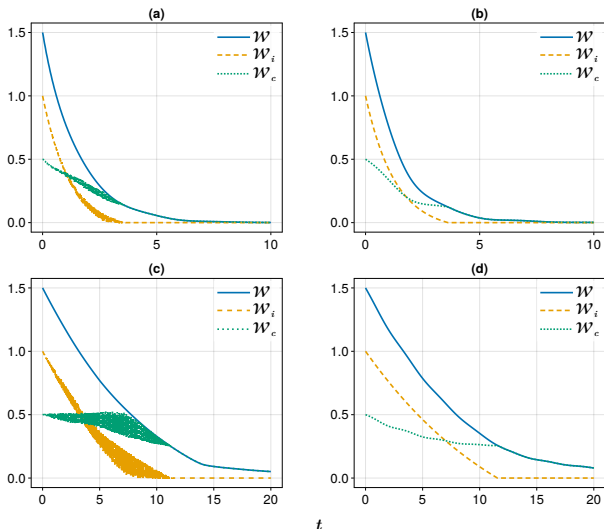


FIG. 5. Ergotropy dynamics with time (in natural units, where $\hbar = k_B = 1$) for the two-qubit collective decoherence quantum battery. The initial two-qubit state is considered a product state $|0+\rangle = \frac{1}{\sqrt{2}}(|00\rangle + |01\rangle)$. (a) and (b) correspond to a squeezed thermal bath at temperature $T = 5$ with squeezing parameters $r = 0.5$ and $\Phi = \frac{\pi}{4}$, while Figures (c) and (d) show the vacuum bath case. Subplots (a) and (c) depict results for $k_0 r_{ij} = 0.1$ (collective decoherence), and (b) and (d) are for $k_0 r_{ij} = 1.2$ (independent dissipation). The other parameters are: $\omega_1 = \omega_2 = 1.0$, $\mu r_{ij} = 0$, $\Gamma_1 = \Gamma_2 = 0.05$.

with DM interaction.

B. Two-qubit collective decoherence battery

Here, we analyze the performance of the two-qubit collective decoherence quantum battery, see Sec. II B 2. In Fig. 5, we discuss the time evolution of ergotropy considering the effects of both the bath and interatomic distance. Both the coherent and incoherent components contribute to the total ergotropy, see Eq. (4). While the coherent part dominates over longer times, the incoherent contribution decays rapidly and becomes negligible. When the qubits are close enough to experience collective decoherence, revivals appear in both the coherent and incoherent ergotropy. These revivals are synchronized in such a way that the overall ergotropy still exhibits a monotonic decay, as shown in Figs. 5(a) and (c). In contrast, when the qubits undergo independent decoherence, both the (in-)coherent ergotropy decay monotonically, and so does the ergotropy. Further, a comparison between different bath conditions highlights the role of temperature. Under the influence of the squeezed thermal bath, the ergotropy decays faster than that in the vacuum bath case due to the finite effective temperature of the squeezed bath, which accelerates the dissipation of extractable work.

Furthermore, we analyze the effect of interatomic distance on the evolution of ergotropy for qubits initially prepared in a Bell state. As shown in Figs. 6(a) and (b), the total ergotropy, including both coherent and incoherent contri-

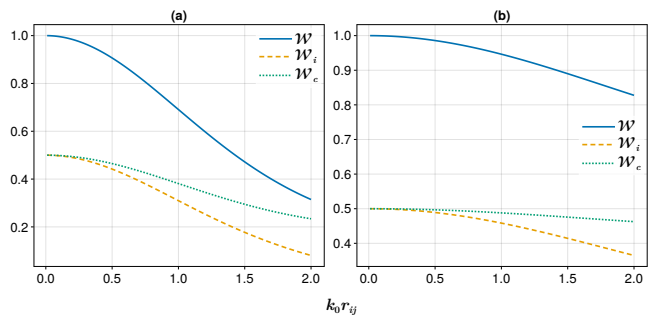


FIG. 6. Variation of ergotropy with the interatomic distance r_{ij} at a given time $t = 2$ for the two-qubit collective decoherence battery. The initial state of the two qubits is taken to be the Bell-state $\frac{1}{\sqrt{2}}(|01\rangle - |10\rangle)$. The squeezed thermal bath parameters are: (a) $T = 5$, $r = 0.5$, $\Phi = \frac{\pi}{4}$, and (b) $T = 0.4$, $r = 0.5$, $\Phi = \frac{\pi}{4}$. Further, $\omega_1 = \omega_2 = 1.0$, $\mu r_{ij} = 0$, $\Gamma_1 = \Gamma_2 = 0.05$. Natural units are taken, where $\hbar = k_B = 1$.

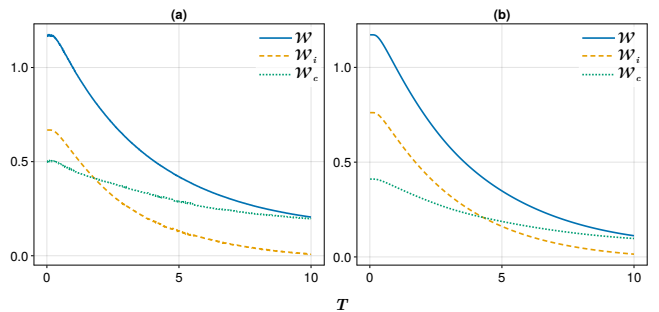


FIG. 7. Variation of ergotropy with temperature for the 2-qubit system in interaction with a squeezed thermal bath at time $t = 2$ with squeezing parameters $r = 0.5$ and $\Phi = \frac{\pi}{4}$. (a) depicts results for $k_0 r_{ij} = 0.05$ (collective decoherence) and (b) for $k_0 r_{ij} = 1.1$ (independent dissipation). The other parameters are: $\omega_1 = \omega_2 = 1.0$, $\mu r_{ij} = 0$, $\Gamma_1 = \Gamma_2 = 0.05$. Natural units are taken, where $\hbar = k_B = 1$.

butions, decreases very slowly under collective decoherence ($r_{ij} \leq 1$), particularly at low temperature, see Fig. 6(b) where it remains nearly stationary. In contrast, for independent decoherence ($r_{ij} \geq 1$), the amount of extractable work from the battery decays faster as the incoherent part vanishes quickly, while the coherent part continues to contribute but also diminishes with time. Notably, in the low temperature case, Fig. 6(b), the decay of ergotropy is slower compared to the high-temperature case in Fig. 6(a).

In Fig. 7, we examine the dependence of ergotropy on temperature for both the collective and independent coherence, with the battery qubits initially prepared in the product state $|0+\rangle$. As shown in Figs. 7(a) and (b), increasing temperature enhances the dissipation of ergotropy into the environment, thereby reducing the amount of extractable work. For collective decoherence, the coherent contribution remains larger than in the case of independent decoherence, resulting in a comparatively slower decay of the total ergotropy.

In Figs. 5 and 7, the initial dominance of the incoherent er-

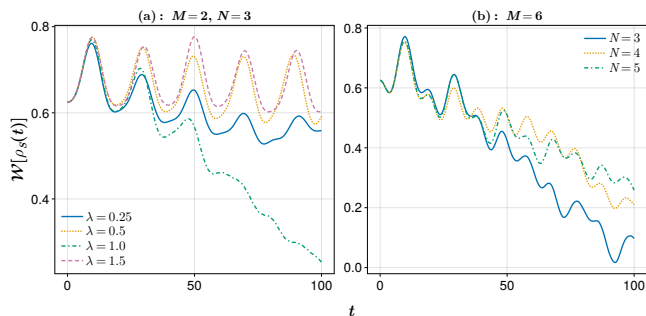


FIG. 8. Variation of the ergotropy with time for the two central spin charger-battery model for different λ in (a), and for different number of bath spins interacting with the charger in (b) at $\lambda = 1.0$. The parameters are: $\omega_C = 1.5$, $\omega_B = 1.25$, $g_{CB} = 0.05$, $g_{CEC} = 0.04$, $g_{BEB} = 0.02$, $\omega_{EB} = 0.6$, $\omega_{EC} = 0.7$, $\gamma = 1$, $T_C = 0.5$, $T_B = 0.8$. In (a), $M = 2$, $N = 3$, and in (b) $M = 6$. Natural units are taken, where $\hbar = k_B = 1$.

gotropy is due to the initial state of the system. Further, due to dissipation of the higher-energy population terms, the incoherent ergotropy drops rapidly. However, the coherence of the system remains, responsible for the crossover. At longer duration and higher temperatures, the coherent ergotropy becomes the overall ergotropy of the system.

IV. TWO CENTRAL SPINS AS CHARGER AND BATTERY

Here, the two central spins are considered in a charger-battery setup, with one modeled as a charging qubit and the other as a battery qubit, see Eq. (24) and Sec. II B 3. The charging central spin is coupled to an anisotropic spin-1/2 XY chain, whereas the battery is interacting with a spin bath of non-interacting qubits. For simplicity, we set $\gamma = 1$; in this case, the spin chain becomes the Ising model. For any value of γ , quantum criticality occurs at the critical magnetic field strength $\lambda_c = 1$. It has been shown earlier that the quantum speed limit time (QSLT) has some strong imprint of the quantum phase transition for the XY model, even for a finite-sized environment, and exhibits noticeable anomalous behavior near the critical point, where the non-Markovianity (calculated using the Breuer-Laine-Piilo (BLP) measure [106]) was also shown to be impacted by the phase transition [83]. In order to study the performance of the quantum battery near the critical point, we plot the ergotropy, energy, and power as a function of magnetic field λ and time.

In Fig. 8, the time evolution of the ergotropy of the battery qubit for different values of magnetic field strengths λ is depicted. The ergotropy exhibits an oscillatory behavior. Due to the interaction of the battery with the charger, the ergotropy initially increases, indicating charging of the battery. The ergotropy drops again due to its interaction with the environment, and this cycle continues. An interesting observation is made at the critical point $\lambda_c = 1.0$. At this point, the ergotropy decays rapidly at longer times, which indicates that the environment has a greater impact on its dissipation than

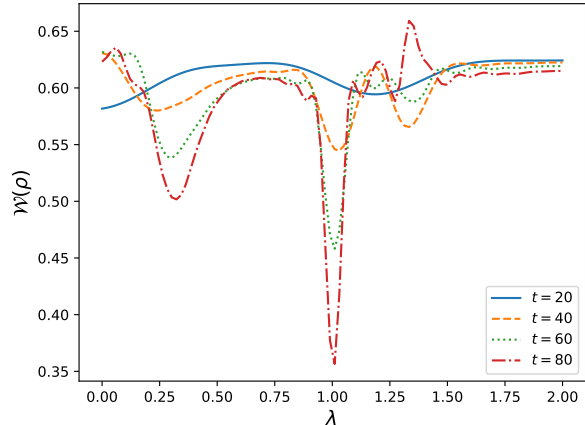


FIG. 9. Variation of the ergotropy with λ for the two central spin charger-battery model at different times. The parameters are: $\omega_C = 1.5$, $\omega_B = 1.25$, $g_{CB} = 0.05$, $g_{CEC} = 0.04$, $g_{BEB} = 0.02$, $\omega_{EB} = 0.6$, $\omega_{EC} = 0.7$, $M = 2$, $N = 3$, $\gamma = 1$, $T_C = 0.5$, $T_B = 0.8$. Natural units are taken, where $\hbar = k_B = 1$.

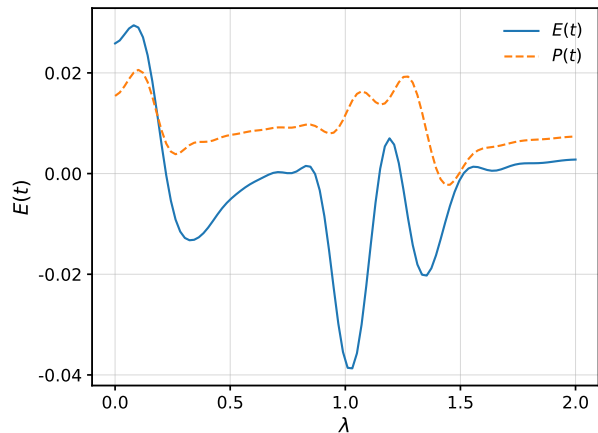


FIG. 10. Variation of the energy and power of battery spin with magnetic field strength λ for the two central spin charger-battery model at time $t = 40$. The parameters are: $\omega_C = 1.5$, $\omega_B = 1.25$, $g_{CB} = 0.05$, $g_{CEC} = 0.04$, $g_{BEB} = 0.02$, $\omega_{EB} = 0.6$, $\omega_{EC} = 0.7$, $M = 2$, $N = 3$, $\gamma = 1$, $T_C = 0.5$, $T_B = 0.8$. Natural units are taken, where $\hbar = k_B = 1$.

its charging via the charger, and the battery almost completely loses the work that can be extracted from it, as ergotropy approaches zero in the long-time limit. The recharging of the battery here could be attributed to the non-Markovian system-bath interactions. At the critical point, this non-Markovian effect is highly suppressed, resulting in critical discharging. In Fig. 8(b) the ergotropy is plotted for a higher number of bath spins interacting with the charger and the battery at the critical coupling, where a consistent behavior of the ergotropy emerges, that is, the ergotropy decreases at the critical coupling and also with the increase in the bath spins.

Further, to investigate the behavior of the battery qubit near

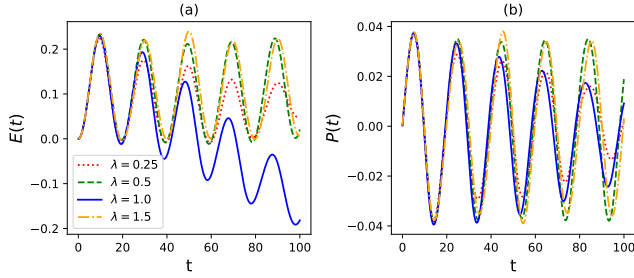


FIG. 11. Variation of the energy $E(t)$ and power $P(t)$ of battery spin with time for the two central spin charger-battery model at different λ . The parameters are: $\omega_C = 1.5$, $\omega_B = 1.25$, $g_{CB} = 0.05$, $g_{CEC} = 0.04$, $g_{BE_B} = 0.02$, $\omega_{E_B} = 0.6$, $\omega_{E_C} = 0.7$, $M = 2$, $N = 3$, $\gamma = 1$, $T_C = 0.5$, $T_B = 0.8$. Natural units are taken, where $\hbar = k_B = 1$.

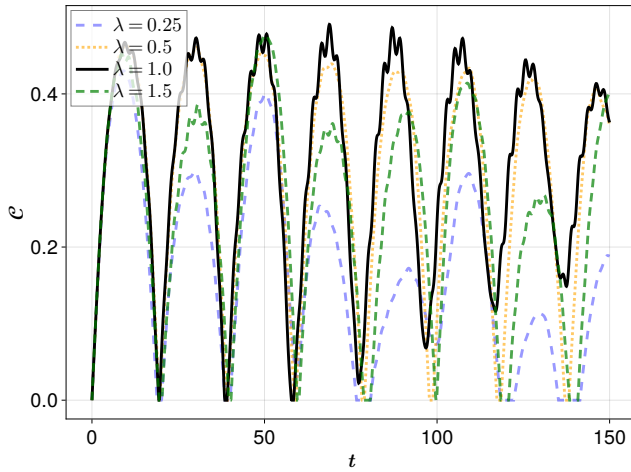


FIG. 12. Variation of the concurrence C of charger-battery spin with time for the two central spin charger-battery model at different λ . The parameters are: $\omega_C = 1.5$, $\omega_B = 1.25$, $g_{CB} = 0.05$, $g_{CEC} = 0.04$, $g_{BE_B} = 0.02$, $\omega_{E_B} = 0.6$, $\omega_{E_C} = 0.7$, $M = 2$, $N = 3$, $\gamma = 1$, $T_C = 0.5$, $T_B = 0.8$. Natural units are taken, where $\hbar = k_B = 1$.

the critical point, we analyze the variation of ergotropy with the magnetic field strength, as shown in Fig. 9. At $t = 20$, the ergotropy profile as a function of the magnetic-field strength is nearly stationary. For longer evolution times, for example, at $t = 40, 60$, and 80 , local minima appear at several λ values, while the ergotropy at large λ values remains close to its earlier time values. However, at the critical point $\lambda_c = 1$, a sharp and pronounced minimum is observed, particularly at longer times, corresponding to the lowest ergotropy and a significantly larger drop than at other λ values.

In Figs. 10 and 11, we discuss the energy and power of the battery with evolution time and magnetic field strength. The time evolution of the energy exhibits behavior similar to that of the ergotropy for different values of λ shown in Fig. 8. The battery qubit loses energy through interactions with the bath and regains it back via the battery-charger coupling. As observed in Fig. 11, the energy and power display qualitatively similar trends for $\lambda = 0.25, 0.5$, and 1.5 . When the system dis-

sipates energy, power becomes negative, whereas energy absorption from the environment corresponds to positive power. Thus, energy and power remain consistent with one another, both showing oscillatory behavior. However, at the critical point, the amplitude of the energy oscillations decreases over longer evolution times, with the energy approaching its minimum attainable value for the battery qubit. Consequently, the power also exhibits damped oscillations. In particular, Fig. 10 illustrates that at $\lambda_c = 1$, during the evolution of energy and power, the energy attains its minimum value at a specific time, highlighting the distinct dynamical response near criticality.

Furthermore, the entanglement between the charger and the battery is studied to better understand the behavior of the battery at the critical point. To this end, we use concurrence C to explore the entanglement between the battery and charger qubit. This charger-battery setup forms a two-qubit bipartite system, in which case, the concurrence of the system is given by

$$C = \max\{0, \lambda_1 - \lambda_2 - \lambda_3 - \lambda_4\}, \quad (25)$$

where λ_i 's are the eigenvalue of the matrix $\sqrt{\sqrt{\rho_{CB}(t)}\tilde{\rho}_{CB}(t)\sqrt{\rho_{CB}(t)}}$ in decreasing order, and $\tilde{\rho}_{CB}(t) = (\sigma_y \otimes \sigma_y)\rho_{CB}^*(t)(\sigma_y \otimes \sigma_y)$. $\rho_{CB}(t)$ is the two-qubit system's density matrix given by Eq. (23). The concurrence is calculated using the above formula, and is plotted in Fig. 12. The figure shows that at critical coupling, entanglement is higher at longer durations. This points out that a reason for less extractable work at the critical coupling could be attributed to a larger entanglement between the charger and the battery.

Up to this point, we have discussed that the battery qubit loses ergotropy due to system-bath interactions, while the battery-charger coupling helps it regain ergotropy, energy, and power. To further understand the charging behavior of the battery qubit, here we analyze the instantaneous charging power and the average (dis-)charging power in Fig. 13. Positive (negative) power indicates charging (discharging), corresponding to an increase (decrease) in ergotropy. In Fig. 13(a) and (b), for $\lambda = 0.25$ and $\lambda = 0.5$, the positive peaks of power cycles are slightly lower than the negative ones, resulting in an average charging power that is somewhat lower than the average discharging. However, at the critical point $\lambda = 1$, shown in Fig 13(c), the positive peaks decay rapidly, while the negative part of the power persists. This behavior is consistent with the earlier observation that ergotropy decays faster at the critical point for long-time evolution. Consequently, compared with other values of λ , the average charging power is significantly decreased, while the average discharging power remains higher, thereby increasing the difference between the two.

So far, we have investigated three distinct models of quantum batteries within an open quantum system framework. In the first two models, a two-qubit battery is considered to study the effect of inter-qubit interaction on battery performance. In the first model, we examined the role of inter-qubit interactions by comparing DM and Heisenberg XXX couplings in a two-qubit battery. In the second model, we investigated

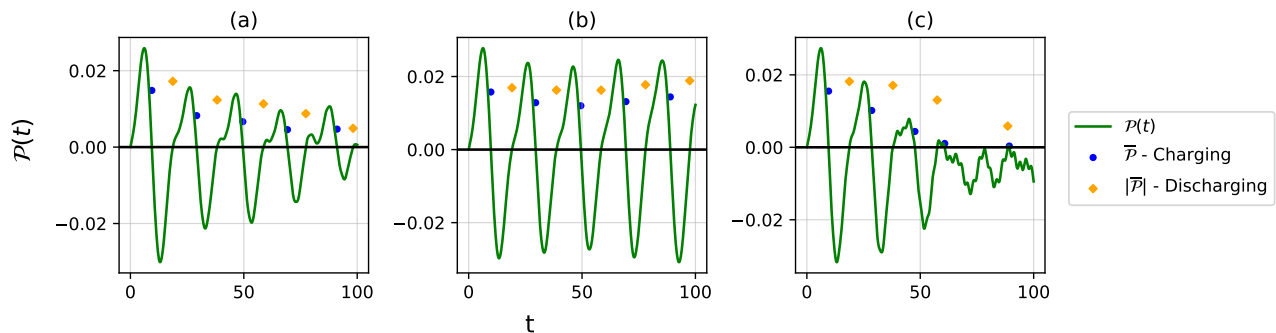


FIG. 13. Variation of instantaneous charging power, average (dis-)charging power of battery spin with time for the two central spin charger-battery model for (a) $\lambda = 0.25$, (b) $\lambda = 0.5$, and (c) $\lambda = 1.0$. The parameters are: $\omega_C = 1.5$, $\omega_B = 1.25$, $\omega_{E_C} = 0.7$, $\omega_{E_B} = 0.6$, $g_{CB} = 0.05$, $g_{CE_C} = 0.04$, $g_{BE_B} = 0.02$, $T_C = 0.5$, and $T_B = 0.8$. Natural units are taken, where $\hbar = k_B = 1$.

the effect of collective decoherence and temperature on extractable work. In both cases, the contribution of coherence to the battery performance was analyzed. Finally, to explore the role of entanglement and quantum criticality, we considered a charger–battery setup in which criticality is introduced through a spin-chain bath coupled to the charger. Together, these models provide a unified perspective on how interactions, environmental effects, coherence, entanglement, and critical behavior govern quantum battery dynamics.

V. CONCLUSIONS

In this work, three two-qubit models have been analyzed for quantum battery applications with distinct features. In the first model, the impact of the inter-qubit interactions, particularly the DM and Heisenberg XXX interaction, on the performance of the quantum battery was investigated. The division of ergotropy into its (in)coherent parts for this model revealed that the incoherent ergotropy was responsible for the dominance of ergotropy in the XXX inter-qubit interaction case. This was further benchmarked by the charging power and average (dis-)charging power, highlighting that XXX inter-qubit interaction fares better at longer duration for work extraction applications.

In the two-qubit collective decoherence model with a

squeezed thermal bath, ergotropy dynamics were governed by interatomic distance and bath temperature. Collective decoherence led to slower decay of the ergotropy, with the coherent component dominating at long times, while independent decoherence resulted in a faster, monotonic loss of extractable work. Higher bath temperatures, in a squeezed thermal bath, accelerated ergotropy dissipation, whereas low-temperature environments helped in preserving it. Overall, collective effects and low temperatures were seen to enhance the longevity of ergotropy, highlighting their crucial role in maintaining the battery’s work-extraction capabilities.

To understand the effect of quantum criticality on battery performance, a two-qubit model composed of a charger and a battery qubit was considered. At the critical point $\lambda_c = 1$, ergotropy decayed rapidly, energy oscillations were damped, and power was predominantly negative, indicating that the environmental effects dominated over charging. The entanglement between the charger and the battery qubits was higher at the critical coupling and at longer durations, suggesting that higher entanglement between the charger and the battery may lead to lower work extraction from the battery. Furthermore, at critical coupling, the instantaneous and average charging powers were significantly reduced, while discharging persisted, resulting in minimal extractable work. These results suggest that criticality strongly suppresses the long-time performance of the central spin quantum battery.

-
- [1] J. Gemmer, M. Michel, and G. Mahler, *Quantum Thermodynamics: Emergence of Thermodynamic Behavior Within Composite Quantum Systems*, Lecture Notes in Physics (Springer Berlin Heidelberg, 2004).
- [2] F. Binder, L. Correa, C. Gogolin, J. Anders, and G. Adesso, *Thermodynamics in the Quantum Regime: Fundamental Aspects and New Directions*, Fundamental Theories of Physics (Springer International Publishing, 2019).
- [3] S. Vinjanampathy and J. Anders, *Contemporary Physics* **57**, 545 (2016), <https://doi.org/10.1080/00107514.2016.1201896>.
- [4] S. Deffner, S. Campbell, I. of Physics (Gran Bretanya), and M. . C. Publishers, *Quantum Thermodynamics: An Introduction to the Thermodynamics of Quantum Information*, IOP (Series): Release 6 (Morgan & Claypool Publishers, 2019).
- [5] U. Seifert, *Reports on Progress in Physics* **75**, 126001 (2012).
- [6] P. Talkner and P. Hänggi, *Rev. Mod. Phys.* **92**, 041002 (2020).
- [7] K. Sekimoto, *Stochastic Energetics*, Lecture Notes in Physics (Springer Berlin Heidelberg, 2010).
- [8] R. Alicki and R. Kosloff, Introduction to quantum thermodynamics: History and prospects, in *Thermodynamics in the Quantum Regime: Fundamental Aspects and New Directions*, edited by F. Binder, L. A. Correa, C. Gogolin, J. Anders, and G. Adesso (Springer International Publishing, Cham, 2018) pp. 1–33.

- [9] G. T. Landi and M. Paternostro, *Rev. Mod. Phys.* **93**, 035008 (2021).
- [10] D. Tiwari, B. Bose, and S. Banerjee, *The Journal of Chemical Physics* **162**, 114104 (2025).
- [11] S. Banerjee, S. Choudhury, S. Chowdhury, J. Knaute, S. Panda, and K. Shirish, *Nuclear Physics B* **996**, 116368 (2023).
- [12] N. Pathania, D. Tiwari, and S. Banerjee, *Quantum Information Processing* **24**, 290 (2025).
- [13] G. Gour, *PRX Quantum* **3**, 040323 (2022).
- [14] R. Alicki, *Journal of Physics A: Mathematical and General* **12**, L103 (1979).
- [15] G. Thomas, N. Siddharth, S. Banerjee, and S. Ghosh, *Phys. Rev. E* **97**, 062108 (2018).
- [16] A. Kumar, S. Lahiri, T. Bagarti, and S. Banerjee, *Physica A: Statistical Mechanics and its Applications* **623**, 128832 (2023).
- [17] G. Watanabe, B. P. Venkatesh, P. Talkner, M.-J. Hwang, and A. del Campo, *Phys. Rev. Lett.* **124**, 210603 (2020).
- [18] D. Tiwari, S. Bhattacharya, and S. Banerjee, *Phys. Rev. Lett.* **135**, 020404 (2025).
- [19] J. Ordonez-Miranda, Y. Ezzahri, and K. Joulain, *Phys. Rev. E* **95**, 022128 (2017).
- [20] K. Joulain, J. Drevillon, Y. Ezzahri, and J. Ordonez-Miranda, *Phys. Rev. Lett.* **116**, 200601 (2016).
- [21] N. Gupt, S. Bhattacharyya, B. Das, S. Datta, V. Mukherjee, and A. Ghosh, *Phys. Rev. E* **106**, 024110 (2022).
- [22] K. Poulsen, A. C. Santos, and N. T. Zinner, *Phys. Rev. Lett.* **128**, 240401 (2022).
- [23] F. Campaioli, S. Gherardini, J. Q. Quach, M. Polini, and G. M. Andolina, *Rev. Mod. Phys.* **96**, 031001 (2024).
- [24] G. M. Andolina, M. Keck, A. Mari, M. Campisi, V. Giovannetti, and M. Polini, *Phys. Rev. Lett.* **122**, 047702 (2019).
- [25] D. Farina, G. M. Andolina, A. Mari, M. Polini, and V. Giovannetti, *Phys. Rev. B* **99**, 035421 (2019).
- [26] D. Tiwari and S. Banerjee, *Frontiers in Quantum Science and Technology* **2**, 1207552 (2023).
- [27] G. Bhanja, D. Tiwari, and S. Banerjee, *Phys. Rev. A* **109**, 012224 (2024).
- [28] M. Yadav, D. Tiwari, and S. Banerjee, *Advanced Quantum Technologies* **n/a**, e00333.
- [29] G. M. Andolina, V. Stanzione, V. Giovannetti, and M. Polini, *Phys. Rev. Lett.* **134**, 240403 (2025).
- [30] R. Shastri, C. Jiang, G.-H. Xu, B. Prasanna Venkatesh, and G. Watanabe, *npj Quantum Information* **11**, 9 (2025).
- [31] D. Rinaldi, R. Filip, D. Gerace, and G. Guarnieri, *Phys. Rev. A* **112**, 012205 (2025).
- [32] R. Alicki and M. Fannes, *Phys. Rev. E* **87**, 042123 (2013).
- [33] F. C. Binder, S. Vinjanampathy, K. Modi, and J. Goold, *New Journal of Physics* **17**, 075015 (2015).
- [34] F. Campaioli, F. A. Pollock, and S. Vinjanampathy, Quantum batteries - review chapter (2018), [arXiv:1805.05507](https://arxiv.org/abs/1805.05507) [quant-ph].
- [35] F. Campaioli, F. A. Pollock, F. C. Binder, L. Céleri, J. Goold, S. Vinjanampathy, and K. Modi, *Phys. Rev. Lett.* **118**, 150601 (2017).
- [36] J.-Y. Gyhm and U. R. Fischer, *AVS Quantum Science* **6**, 012001 (2024).
- [37] D. Ferraro, M. Campisi, G. M. Andolina, V. Pellegrini, and M. Polini, *Phys. Rev. Lett.* **120**, 117702 (2018).
- [38] F.-Q. Dou, Y.-Q. Lu, Y.-J. Wang, and J.-A. Sun, *Phys. Rev. B* **105**, 115405 (2022).
- [39] T. P. Le, J. Levinsen, K. Modi, M. M. Parish, and F. A. Pollock, *Phys. Rev. A* **97**, 022106 (2018).
- [40] J.-X. Liu, H.-L. Shi, Y.-H. Shi, X.-H. Wang, and W.-L. Yang, *Phys. Rev. B* **104**, 245418 (2021).
- [41] D. Rossini, G. M. Andolina, D. Rosa, M. Carrega, and M. Polini, *Phys. Rev. Lett.* **125**, 236402 (2020).
- [42] W.-L. Song, J.-L. Wang, B. Zhou, W.-L. Yang, and J.-H. An, *Phys. Rev. Lett.* **135**, 020405 (2025).
- [43] F.-M. Yang and F.-Q. Dou, *Phys. Rev. A* **109**, 062432 (2024).
- [44] W.-X. Guo, F.-M. Yang, and F.-Q. Dou, *Phys. Rev. A* **109**, 032201 (2024).
- [45] Z.-G. Lu, G. Tian, X.-Y. Lü, and C. Shang, *Phys. Rev. Lett.* **134**, 180401 (2025).
- [46] A. Mukherjee, S. Gangopadhyay, and A. S. Majumdar, Enhancement of an unruh-dewitt battery performance through quadratic environmental coupling (2024), [arXiv:2411.02849](https://arxiv.org/abs/2411.02849) [gr-qc].
- [47] A. E. Allahverdyan, R. Balian, and T. M. Nieuwenhuizen, *Europhysics Letters* **67**, 565 (2004).
- [48] W. Pusz and S. L. Woronowicz, *Communications in Mathematical Physics* **58**, 273 (1978).
- [49] G. Francica, F. C. Binder, G. Guarnieri, M. T. Mitchison, J. Goold, and F. Plastina, *Phys. Rev. Lett.* **125**, 180603 (2020).
- [50] B. Çakmak, *Phys. Rev. E* **102**, 042111 (2020).
- [51] F. H. Kamin, F. T. Tabesh, S. Salimi, F. Kheirandish, and A. C. Santos, *New Journal of Physics* **22**, 083007 (2020).
- [52] A. H. Malavazi, R. Sagar, B. Ahmadi, and P. R. Dieguez, *PRX Energy* **4**, 023011 (2025).
- [53] A. H. A. Malavazi, B. Ahmadi, P. Horodecki, and P. R. Dieguez, Charge-preserving operations in quantum batteries (2025), [arXiv:2510.25549](https://arxiv.org/abs/2510.25549) [quant-ph].
- [54] B. Ahmadi, P. Mazurek, P. Horodecki, and S. Barzanjeh, *Phys. Rev. Lett.* **132**, 210402 (2024).
- [55] B. Ahmadi, A. B. Ravichandran, P. Mazurek, S. Barzanjeh, and P. Horodecki, [arXiv:2510.06384](https://arxiv.org/abs/2510.06384) (2025).
- [56] B. Ahmadi, P. Mazurek, S. Barzanjeh, and P. Horodecki, *Phys. Rev. Appl.* **23**, 024010 (2025).
- [57] H. Breuer and F. Petruccione, *The Theory of Open Quantum Systems* (Oxford University Press, 2002).
- [58] U. Weiss, *Quantum Dissipative Systems*, 4th ed. (WORLD SCIENTIFIC, 2012).
- [59] S. Banerjee, *Open Quantum Systems: Dynamics of Nonclassical Evolution*, 1st ed. (Springer Publishing Company, Incorporated, 2018).
- [60] V. Gorini, A. Kossakowski, and E. C. G. Sudarshan, *Journal of Mathematical Physics* **17**, 821 (2008).
- [61] G. Lindblad, *Communications in Mathematical Physics* **48**, 119 (1976).
- [62] I. de Vega and D. Alonso, *Rev. Mod. Phys.* **89**, 015001 (2017).
- [63] L. Li, M. J. Hall, and H. M. Wiseman, *Physics Reports* **759**, 1 (2018), concepts of quantum non-Markovianity: A hierarchy.
- [64] M. J. W. Hall, J. D. Cresser, L. Li, and E. Andersson, *Phys. Rev. A* **89**, 042120 (2014).
- [65] Ángel Rivas, S. F. Huelga, and M. B. Plenio, *Reports on Progress in Physics* **77**, 094001 (2014).
- [66] D. Chruściński, *Physics Reports* **992**, 1 (2022), dynamical maps beyond Markovian regime.
- [67] S. Utagi, R. Srikanth, and S. Banerjee, *Scientific Reports* **10**, 15049 (2020).
- [68] C. Käding and M. Pitschmann, Density matrices in quantum field theory: Non-markovianity, path integrals and master equations (2025), [arXiv:2503.08567](https://arxiv.org/abs/2503.08567) [hep-th].
- [69] D. Morrone, M. A. C. Rossi, A. Smirne, and M. G. Genoni, *Quantum Science and Technology* **8**, 035007 (2023).
- [70] A. Caldeira and A. Leggett, *Annals of Physics* **149**, 374 (1983).

- [71] A. J. Leggett, S. Chakravarty, A. T. Dorsey, M. P. A. Fisher, A. Garg, and W. Zwerger, *Rev. Mod. Phys.* **59**, 1 (1987).
- [72] N. V. Prokof'ev and P. C. E. Stamp, *Reports on Progress in Physics* **63**, 669 (2000).
- [73] N. V. Prokof'ev and P. C. E. Stamp, *Journal of Low Temperature Physics* **104**, 143 (1996).
- [74] J. F. Haase, A. Smirne, J. Kołodyński, R. Demkowicz-Dobrzański, and S. F. Huelga, *New Journal of Physics* **20**, 053009 (2018).
- [75] R. Hanson, F. M. Mendoza, R. J. Epstein, and D. D. Awschalom, *Phys. Rev. Lett.* **97**, 087601 (2006).
- [76] J. I. Cirac and P. Zoller, *Phys. Rev. Lett.* **74**, 4091 (1995).
- [77] J. Joshi and T. S. Mahesh, *Phys. Rev. A* **106**, 042601 (2022).
- [78] H.-P. Breuer, D. Burgarth, and F. Petruccione, *Phys. Rev. B* **70**, 045323 (2004).
- [79] S. Bhattacharya and S. Banerjee, *Quanta* **10**, 55–64 (2021).
- [80] C. Mukhopadhyay, S. Bhattacharya, A. Misra, and A. K. Pati, *Phys. Rev. A* **96**, 052125 (2017).
- [81] D. Tiwari, S. Datta, S. Bhattacharya, and S. Banerjee, *Phys. Rev. A* **106**, 032435 (2022).
- [82] D. Tiwari, K. G. Paulson, and S. Banerjee, *Annalen der Physik* **535**, 2200452 (2023).
- [83] J. Wei, Yong-Bonand Zou, Z.-M. Wang, and B. Shao, *Scientific Reports* **6**, 19308 (2016).
- [84] S. Sachdev, *Quantum Phase Transitions* (Cambridge University Press, Cambridge UK, 2011).
- [85] J. Preskill, *Journal of Modern Optics* **47**, 127–137 (2000).
- [86] A. Dutta, G. Aeppli, B. K. Chakrabarti, U. Divakaran, T. F. Rosenbaum, and D. Sen, *Quantum Phase Transitions in Transverse Field Spin Models: From Statistical Physics to Quantum Information* (Cambridge University Press, 2015).
- [87] G. Vidal, J. I. Latorre, E. Rico, and A. Kitaev, *Phys. Rev. Lett.* **90**, 227902 (2003).
- [88] A. Osterloh, L. Amico, G. Falci, and R. Fazio, *Nature* **416**, 608 (2002).
- [89] Z.-G. Yuan, P. Zhang, and S.-S. Li, *Phys. Rev. A* **76**, 042118 (2007).
- [90] T. Moriya, *Phys. Rev.* **120**, 91 (1960).
- [91] I. Dzyaloshinsky, *Journal of Physics and Chemistry of Solids* **4**, 241 (1958).
- [92] S. R. K and S. Muruges, *Physica Scripta* **100**, 015106 (2024).
- [93] X.-L. Zhang, X.-K. Song, and D. Wang, *Advanced Quantum Technologies* **7**, 2400114 (2024).
- [94] S. Bhattacharya, V. B. Sabale, and A. Kumar, *Heisenberg spin chain models for realising quantum battery with the aid of dzyaloshinskii moriya interaction* (2025), arXiv:2508.20529 [quant-ph].
- [95] B. Vigneshwar and R. Sankaranarayanan, *Journal of Physics A: Mathematical and Theoretical* **59**, 015302 (2026).
- [96] J. R. Parkavi, R. Muthuganesan, and V. K. Chandrasekar, *Physica Scripta* **101**, 015102 (2026).
- [97] W. Heisenberg, *Zeitschrift für Physik* **49**, 619 (1928).
- [98] H. Bethe, *Zeitschrift für Physik* **71**, 205 (1931).
- [99] D. C. Mattis, *The theory of magnetism I*, 1981st ed., Springer Series in Solid-State Sciences (Springer, Berlin, Germany, 1981).
- [100] R. I. NEPOMECHIE, *International Journal of Modern Physics B* **13**, 2973 (1999).
- [101] S. Banerjee, V. Ravishankar, and R. Srikanth, *The European Physical Journal D* **56**, 277 (2010).
- [102] S. Banerjee, V. Ravishankar, and R. Srikanth, *Annals of Physics* **325**, 816 (2010).
- [103] Z. Ficek and R. Tanaś, *Physics Reports* **372**, 369 (2002).
- [104] B. n. Mula, E. M. Fernández, J. E. Alvarellos, J. J. Fernández, D. García-Aldea, S. N. Santalla, and J. Rodríguez-Laguna, *Phys. Rev. B* **107**, 075116 (2023).
- [105] A. Fert, M. Chshiev, A. Thiaville, and H. Yang, *Journal of the Physical Society of Japan* **92**, 081001 (2023).
- [106] H.-P. Breuer, E.-M. Laine, and J. Piilo, *Phys. Rev. Lett.* **103**, 210401 (2009).